# Effects of the Combined Addition of Zn and Mg on Corrosion Behaviors of Electropainted AlSi-Based Metallic Coatings Used for Hot-Stamping Steel Sheets

**Si On Kim** [1], **Won Seog Yang** [2] **and Sung Jin Kim** [1],*

1   Department of Advanced Materials Engineering, Sunchon National University, Jungang-ro, Suncheon, Jeonnam 57922, Korea; kzo1102@scnu.ac.kr
2   R&D Division, Hyundai Steel, 1480 Bukbusaneop-ro, Songak-eup, Dangjin, Chungnam 31719, Korea; wsyang@hyundai-steel.com
*   Correspondence: sjkim56@sunchon.ac.kr; Tel.: +82-61-750-3557

check for updates

**Abstract:** The effects of the combined addition of Zn and Mg on the corrosion resistance of AlSi-based coating for automotive steel sheets were investigated using a variety of analytical and electrochemical techniques. The preferential dissolution of Mg and Zn from $MgZn_2$/$Mg_2Si$ phases occurred on the AlSi-based coating that had been alloyed with a smaller portion of Zn and Mg, which contributed to the rapid surface coverage by corrosion products with a protective nature, reducing the corrosion current density. On the other hand, localized corrosion attacks caused by the selective dissolution of Mg were also observed in the AlSi-based coating with a smaller portion of Zn and Mg. Such alloying can also worsen its corrosion resistance when coated additionally with electrodeposited paint. The mechanistic reasons for these conflicting results are also discussed.

**Keywords:** hot stamping steel; AlSi-based coating; electrodeposited paint; Zn; Mg; corrosion

## 1. Introduction

Metallic coatings have been applied widely to steel substrates used in the automotive industry, because of their anti-corrosion performance [1–3]. In general, coating materials are more electrochemically active than protected substrates, meaning they offer sacrificial protection. A recent technical issue in a coating system is the formation of suitable corrosion products and new phases that are effective in delaying the coating consumption and reducing the overall corrosion rate [4–6]. Regarding Al-based coatings for steel sheets, a passive film ($Al_2O_3$) forms on the coating surface, providing superior barrier protection [7–9]. In the case of AlSi-based coatings, the addition of Si decreases the thickness of the intermetallic phase at the inter-diffusion layer close to the steel substrates [10,11], which also provide good anti-corrosion performance [12]. On the other hand, $Al_2O_3$ films are unstable when exposed to environments containing chloride ions ($Cl^-$), which can decrease the stability of the film, leading to a decrease in coating efficiency by localized corrosion [13,14]. To overcome these drawbacks, other alloying elements, such as Zn and Mg, which can modify the coating potential, are added to the Al-based coating, so that they can provide a supplementary self-healing effect by the sacrificial dissolution of alloying elements [4,5]. At the same time, several corrosion products acting as a protective barrier can be formed on the outer surface [15,16]. Hence, AlSi-based coatings with Zn and Mg are promising candidates for metallic coatings on hot-stamping steels used for auto-parts [17]. Recently, Nicard et al. [18] examined the anti-corrosion mechanism of AlSi-based coatings with Zn (2~30 wt %) and Mg (1~10 wt %). They reported that the addition of Zn and Mg to AlSi-based coatings increases the corrosion resistance in chloride-containing environments. From a practical and an industrial point of view, however, lower concentrations of Zn and Mg, which have low

melting temperatures, are favored to avoid the liquid metal embrittlement (LME) phenomenon [19] and localized corrosion attack caused by the selective dissolution of these alloying elements [6,20].

Furthermore, considering the applicability of the coating to hot-stamped, high strength steel sheets used for auto-body parts, an evaluation of the corrosion resistance should proceed after the electropainting process on the metallic coating. In this regard, this study examined on the corrosion behaviors not only of AlSi-based metallic coating with 10 wt % Zn and 0.5 wt % Mg (refer to AlSiZnMg-MC, here-in-after), but also of electropainted AlSiZnMg-MC. Field-emission scanning electron microscopy (FE-SEM), X-ray diffraction (XRD), X-ray photoelectron spectroscopy (XPS), and potentiostat measurements were used to analyze the corrosion behaviors of metallic coated steels. Moreover, an accelerated corrosion test [12] was conducted on electropainted samples that had been damaged by scratching the coating with an "×" incision, and by colliding the coating surface with fine stone.

## 2. Experimental

### 2.1. Materials and Specimen Preparation

The steel substrate, produced by Hyundai Steel Corp.(Dang Jin, Korea), was classified as 22MnB5 steel with 0.27–0.3 wt % C, 1.3–1.5 wt % Mn, 0.2–0.25 wt % Cr, 0.18–0.2 wt % Si, 0.0025–0.0035 wt % B, 0.02–0.035 wt % Ti. The S and P contents were kept as low as possible to avoid high-temperature cracking during the subsequent stamping process. Two types of metallic coated steel were used: AlSi and AlSi with Zn and Mg (AlSiZnMg) coated steels, which were manufactured using a hot-dip simulator. For the coating process, two types of molten bath were prepared: Al-Si (7 wt %) and Al-Si (7 wt %)-Zn (10 wt %)–Mg (0.5 wt %). The substrates were then dipped in each molten bath, and two types of metallic coating were produced: AlSi-MC and AlSiZnMg-MC, at 50/50 g/m$^2$. For the following stamping process, the two metallic coated steels were heated to 930 °C for 300 s and cooled to room temperature by die quenching.

Some of the two types of metallic coated steel sample were also coated with electrodeposited (ED) paint. For this ED coating, the coated steel samples underwent the following processes: degreasing, surface conditioning, and phosphating in a pretreatment simulator. The ED coating was then conducted at 300 V for 180 s while the voltage was increased uniformly for 30 s. The ED coated samples were dried in a circulating oven at 170 °C for 20 min. Detailed information on the ED coating process can be found elsewhere [21].

### 2.2. Microstructure Examination

The microstructure and composition of the coated steel samples before and after the corrosion test (potentiostatic (PS) polarization measurement) were examined by FE-SEM and energy dispersive spectroscopy (EDS). Before the corrosion test, the coated steel samples were cleaned ultrasonically in ethanol and dried in air. In particular, for the cross-sectional observations, the samples were mounted with the cut-edge sides facing the surface, and they were polished with a final polishing step of 0.04 µm. After the corrosion test, the sample surface was washed with distilled water and dried in air. The sample was then stored in a vacuum chamber. The various phases in the coating layers were also characterized by XRD.

### 2.3. Depth Profile Analysis

The compositional distributions of the coating layers as a function of depth were examined by glow discharge spectroscopy (GDS) analysis with a Leco (St. Joseph, MI, USA) GDS-850A spectrometer using argon plasma equipped with an RF lamp. The diameter of the analysis area in a sampling area of $20 \times 20$ mm$^2$ was 4 mm.

### 2.4. X-ray Photoelectron Spectroscopy Analysis

XPS was used to analyze the chemical state of the corrosion products formed on the metallic-coated layers after the corrosion test (PS polarization measurement). Prior to analysis, the two types of coated steel sheets that had been corroded by the polarization test were cut into $7 \times 8$ mm$^2$ samples and cleaned using ethanol. XPS (VG Scientific Escalab 250 (Waltham, MA, USA)) was conducted using mono chromatic Al K$\alpha$ radiation (1486.7 eV) with a 500 µm diameter spot size. A constant analyzer energy mode with 200 and 50 eV for the survey and high-resolution spectra, respectively, were used. Data processing of the spectra was performed using a spectral data processor (SDP) v 3.0 software. The adventitious C 1s peak at 284.8 eV was used as a reference for charge correction [22].

### 2.5. Electrochemical Measurements

Potentiodynamic and potentiostatic polarization tests were performed after the open circuit potential (OCP) evolution measurements for 1 h in a 3.5% NaCl using a GAMRY (Philadelphia, PA, USA) reference 600. A three-electrode system was used, which consisted of the metallic-coated sample as the working electrode (tested area of 1 cm$^2$), a platinum grid as the counter electrode, and a saturated calomel electrode (SCE) as the reference electrode.

For the potentiodynamic polarization scan, the working electrode was polarized from −0.5 V to 0.25 V vs. OCP at a scan rate of 0.16 mV s$^{-1}$. The corrosion current densities were determined by curve-fitting using the Wagner-Traud equation (Equation (1)), described below, to the potentiodynamic polarization curves.

$$i = i_{corr}\left[ exp\left( \frac{2.303(E - E_{corr})}{\beta_a} \right) - exp\left( \frac{-2.303(E - E_{corr})}{\beta_c} \right) \right] \qquad (1)$$

where $i_{corr}$ is the corrosion current density (A/cm$^2$), $E_{corr}$ and $E$ represent the corrosion potential (V) and the measured potential (V), respectively. $\beta_a$ and $\beta_c$ are Tafel slopes (V/decade), and $i$ is the total corrosion density (A/cm$^2$).

Based on the polarization curves, the applied potentials for the anodic and cathodic polarization during the potentiostatic polarization measurements were determined to be 50 mV above the OCP and 100 mV below the OCP, respectively. A preliminary test showed that under an applied potential of 100 mV above the OCP in the potentiostatic polarization, the coating dissolution was too severe to analyze the corrosion behaviors of the coating surface covered with some corrosion products. Therefore, the anodic potential was set to 50 mV lower than the cathodic potential in the polarization measurements.

Three repetitive tests were conducted for each experiment to ensure reproducibility.

### 2.6. Cyclic Corrosion Test for ED Coated Samples

To evaluate the corrosion resistance of the ED coated AlSi and AlSiZnMg samples, a VDA (Berlin, Germany) 233-102 cyclic corrosion test was conducted according to VDA 233-102 [12], which is a standard for the accelerated corrosion testing of coatings/paintings within the automotive industry. Before the corrosion test, the samples were cut to a size of $150 \times 70$ mm, and damaged artificially using the following two methods. One set of samples was scratched with an "×" incision in reference to ASTM D-1654 [23], and the other set of samples abraded with a spray of fine stone chips, as reported elsewhere [24]. Salt spraying with a 1% NaCl solution (pH 6.5) at a rate of 2.0 to 4.0 mL/h was then conducted on the samples positioned 65° to the horizontal in an enclosed chamber. A full test cycle lasted for seven days, and the multi-step cycles were composed of varying temperatures ranging from −15 °C to 50 °C and humidity between 50% and 95%. Further information on test conditions can be found in VDA 233-102 [12].

## 3. Results and Discussion

### 3.1. Microstructure Characterizations of Metallic Coatings

Figure 1 presents the surface and cross-sectional morphologies and EDS mapping of AlSi-MC (Figure 1a,b) and AlSiZnMg-MC (Figure 1c,d). EDS mapping showed that the two types of coating were composed mainly of Al matrix with two (Al,Fe,Si)-rich intermetallic phases. One of the intermetallic phases formed at the interface between the coating layer and Fe substrate during the hot-dip aluminizing process. The other phases formed in the coating layer during the austenitizing process. The formation of the former phase was attributed to the inter-diffusion of Fe atoms from the steel substrate into the coating and of Al atoms from the coating into the steel substrate [25]. At the same time, Si, known to be concentrated at the outer surface of the steel substrate [26], was also enriched at the inter-diffusion layer. According to previous studies [27,28], the composition of the intermetallic phase is close to τ5 or τ6 shown in the ternary phase diagram of Al-Fe-Si [27,28]. The latter phase was formed by the diffusion of Fe and Si atoms from the steel substrate into the coating during austenitizing for the hot-stamping process, as reported elsewhere [29]. A noticeable feature in the coating morphologies was the presence of micro-cracks and pores. These may be closely associated with the very high hardness (900~1100 HV0.05) of Al-rich Al-Fe intermetallic compounds, such as $Al_{13}Fe_4$ and $Al_5Fe_2$ [30,31], and the difference in thermal shrinkage among the intermetallic phases during cooling in the hot-stamping process [32].
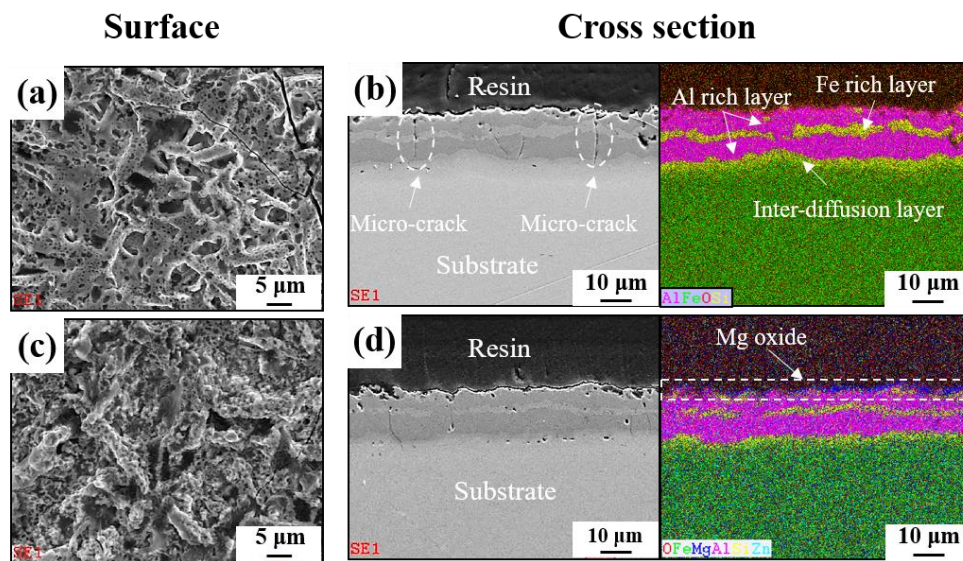


**Figure 1.** Surface and cross-sectional observations with eds mappings of (**a**,**b**) AlSi-MC and (**c**,**d**) AlSiZnMg-MC.

Although Figure 1 indicated that there were more pores and micro-cracks on the AlSi-MC, the microscopic observations could not be representative of the entire coating layers. On the other hand, the composition features were different apparently in that the outer-surface of AlSiZnMg-MC was covered with a thin (Mg, Zn)—based phase. GDS analysis was conducted for further clarification; Figure 2 presents the depth profile results. In contrast to the surface of AlSi-MC, consisting only of a thin Al-based oxide, the Mg and Zn-based oxide may cover the coating layer of AlSiZnMg-MC. In addition, based on the AlSiZnMg quaternary system [33], Zn-Mg intermetallic phases may exist on the coating surface of AlSiZnMg. For closer analysis, phase characterization was carried out using XRD; the results are shown in Figure 3. As expected, one of the major phases in both coating systems was an Al-Fe intermetallic compound.
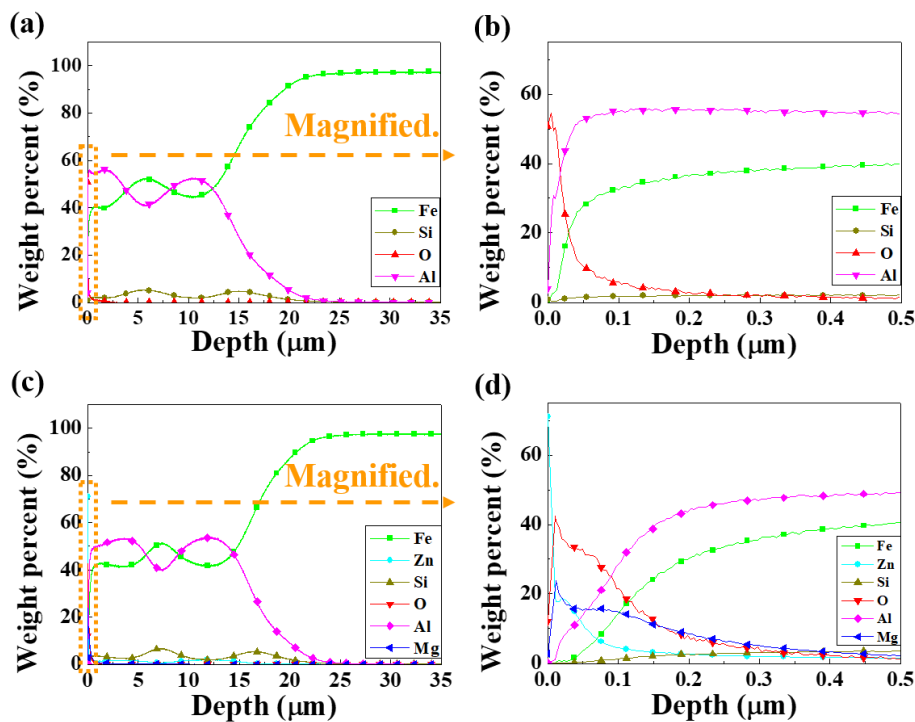
**Figure 2.** Glow discharge spectroscopy (GDS) depth profile of the coating layers: (**a**,**b**) AlSi-MC, (**c**,**d**) AlSiZnMg-MC.
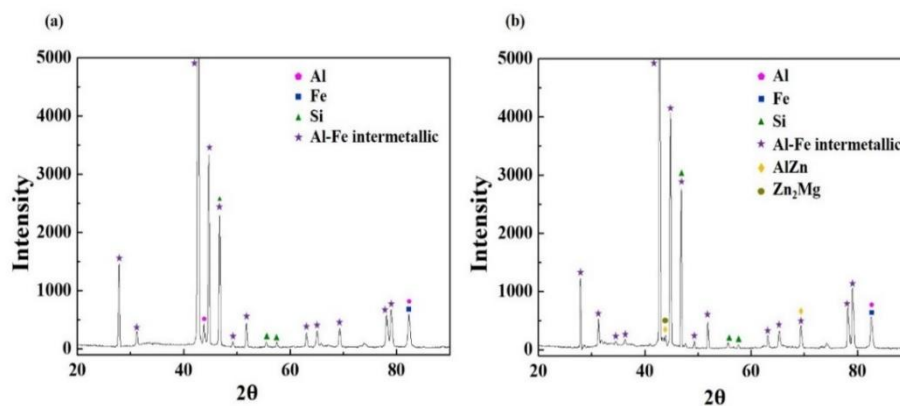


**Figure 3.** X-ray diffraction patterns of (**a**) AlSi-MC and (**b**) AlSiZnMg-MC.

Al-Fe, Fe-Si, and Fe-Al-Si intermetallic phases are generally difficult to distinguish by XRD due to overlap of the XRD peaks [12]. The phase existing only in AlSiZnMg-MC was $MgZn_2$. The other possible phases in the sample may be $Mg_2Si$ and MgO. However, the initial fraction of Mg (0.5 wt %) was too low to give prominent peaks of Mg-containing phases in the XRD measurements. Even if some Mg-containing phases were formed, minor fractions that are below the detection limit of the XRD instrument, might be present. Instead of Mg-containing phases, some peaks for the Al-Fe intermetallic phase and Si were detected with low intensity. Considering that the phases, such as $MgZn_2$ and $Mg_2Si$, have different electrochemical potentials of their own, they can affect the corrosion kinetics and resulting coating life. From an electrochemistry point of view, the phases of $MgZn_2$ and $Mg_2Si$ can act as an anode from the coating matrix because of their lower corrosion potential ($-1538$ and $-1029$ mV$_{SCE}$, respectively) [18]. On the other hand, unlike the case of $MgZn_2$, which provides sacrificial protection at an early stage of corrosion, $Mg_2Si$ can form Si clusters after the selective dissolution of Mg, which will

be cathodic and cause the localized corrosion attack of an Al-based coating layer. [6,20]. This will be discussed in more detail in the following section.

Another possible phase in AlSiZnMg-MC is MgO, which may be present at the outermost part of the coating surface. Although MgO with low electrical conductivity [34] could contribute in part to the suppression of the cathodic reduction reaction during the early corrosion stage, it is generally non-uniform and, in most cases, increases local corrosion attack. Under this coating composition with a minor fraction of Mg (0.5 wt %), it is extremely difficult to form a stable and uniform MgO film over the coating surface. These discussions were based primarily on the theoretical studies reported elsewhere, and they should be clarified experimentally, which will be discussed in the following section.

## 3.2. Electrochemical Characterizations

The evolution of the OCP (Figure 4) was measured for 1 h before the electrochemical polarization tests. The coating potentials of AlSi-MC and AlSiZnMg-MC after 1 h of immersion were approximately $-0.59$ $V_{SCE}$, and $-0.62$ $V_{SCE}$, respectively. In contrast to the Al coating covered by a thin Al oxide film ($Al_2O_3$), Zn and Mg, which were enriched at the coating surface, rarely form an oxide/hydroxide film with a high passivity coefficient in a neutral solution, which could result in a lower corrosion potential. As mentioned previously, the presence of active phases, such as $Mg_2Si$ and $MgZn_2$, can contribute to the decrease in corrosion potential. On the other hand, the preferential dissolution of Mg from the active phases can provide sacrificial protection. Previous studies [16,35] have shown that Mg and Zn cations, which are supplied by the selective dissolution of $MgZn_2$ (reaction (2)), can also lead to rapid coverage of the coating surface by the precipitation of corrosion products with a protective nature, such as simonkolleite ($Zn_5(OH)_8Cl_2 \cdot H_2O$), which can prevent further corrosion.

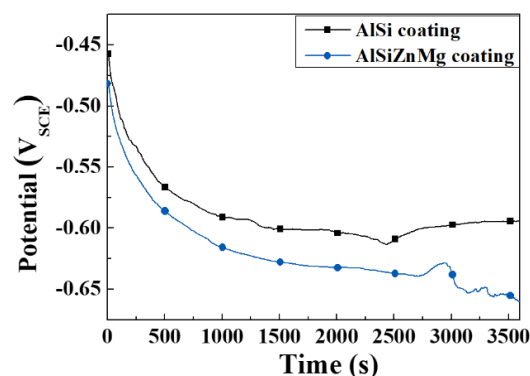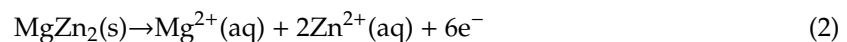$$MgZn_2(s) \rightarrow Mg^{2+}(aq) + 2Zn^{2+}(aq) + 6e^- \tag{2}$$



**Figure 4.** Open circuit potential (OCP) evolution measurement of AlSi-MC and AlSiZnMg-MC for 1 h in a 3.5% NaCl solution [20].

According to a previous study, the selective dissolution of Mg from the $Mg_2Si$ phase can provide cathodic protection. They proposed that the formation of less conductive $SiO_2$ can decrease the galvanic current between Al/$SiO_2$ according to reaction (3) [18,36]:

$$Mg_2Si(s) + 2H_2O(l) \rightarrow 2Mg^{2+}(aq) + SiO_2(s) + 4H^+(aq) + 8e^- \tag{3}$$
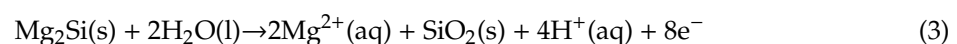
On the other hand, the formation of a stable $SiO_2$ film uniformly formed on the coating surface cannot be guaranteed. Under this condition, an unstable film may create active local galvanic coupling, increasing the dissolution of the coating layer.

These beneficial and harmful effects on the corrosion resistance can be examined by polarization measurements, which are shown in Figure 5; Figure 6. Potentiodynamic and potentiostatic polarizations

showed that the anodic and cathodic reaction rates of AlSiZnMg-MC were much smaller than those of AlSi-MC. The corrosion current densities ($i_{corr}$) determined by curve-fitting with the Wagner–Traud equation to the polarization curves of AlSiZnMg-MC and AlSi-MC were 3.5 and 8.5 μA cm$^{-2}$, respectively. The lower anodic and cathodic current densities of AlSiZnMg-MC suggest that the liberated $Mg^{2+}$ and $Zn^{2+}$ ions, supplied by the selective dissolution of Mg and Zn, provided an environment for the formation of corrosion products contributing to the effective reduction of the anodic and cathodic current densities. On the other hand, the polarization curve of AlSiZnMg-MC has many fluctuations, which may be closely associated with localized corrosion caused by the non-uniform distribution of MgO or the selective dissolution of Mg from $Mg_2Si$ phases in the coating. This can be supported in part by several local corrosion attacks after the corrosion test, as shown in Figure 7. From morphological observations before (Figure 1) and after (Figure 7) the corrosion test (PS polarization), there was little difference except that the outermost surfaces were less uniform after the corrosion test. Compared to the case of AlSi-MC, the surface morphology of AlSiZnMg-MC after the corrosion test appeared to be denser (Figure 7c). On the other hand, AlSiZnMg-MC exhibited a more uneven cross-sectional view, which may be associated with the formation of corrosion products containing Mg, Zn, and Si, and localized corrosion attacks mentioned previously. Owing to the low resolution of EDS or GDS, XPS was performed to characterize the corrosion products formed on the two types of coating after the corrosion test.
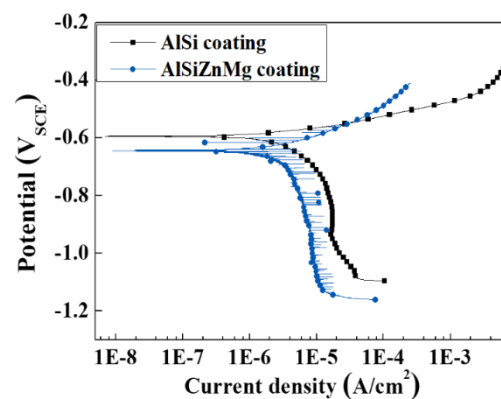


**Figure 5.** Potentiodynamic polarization curves of AlSi-MC and AlSiZnMg-MC, measured after 1 h immersion in a 3.5% NaCl solution [20].
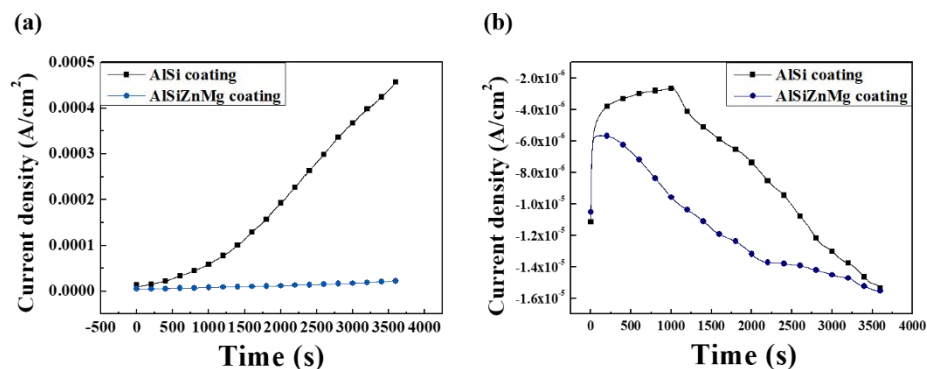


**Figure 6.** Potentiostatic polarization curves of AlSi-MC and AlSiZnMg-MC, measured after 1 h immersion in a 3.5% NaCl solution under (**a**) anodic (50 mV above OCP), and (**b**) cathodic (100 mV below OCP) potentials [20].
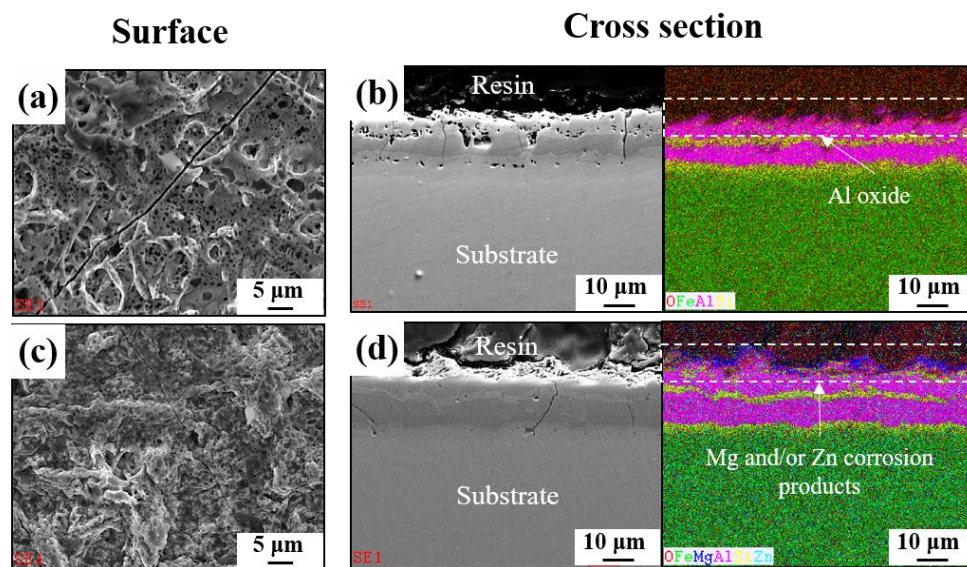
**Surface**

**Cross section**



**Figure 7.** Surface and cross-sectional observations with EDS mappings of (**a**,**b**) AlSi-MC and (**c**,**d**) AlSiZnMg-MC after the potentiostatic (PS) test.

### 3.3. Characterization of the Corrosion Products by XPS

Figure 8 presents the XPS survey spectrum of the surface of AlSi-MC. The spectrum of the coating surface revealed C 1s, Al 2p, O 1s, and Si 2p primarily. The high-resolution spectra, shown in Figure 8c–e, indicated that the corrosion products formed on the surface were composed mainly of $Al_2O_3$ with a smaller portion of $SiO_2$. On the other hand, the survey spectrum of the surface on AlSiZnMg-MC (Figure 9) showed that, in addition to C 1s, Al 2p, O 1s, and Si 2p, Mg 2p and Zn 2p were observed on the coating surface, and the oxygen intensity was higher. This suggests that Zn and Mg-based oxide/hydroxide are major components in the coating surface. From the high-resolution spectra of the surface on AlSiZnMg-MC, as shown in Figure 9c–g, the coating surface was composed of a wider variety of corrosion products including $Al_2O_3$, $Mg(OH)_2$, $SiO_2$, $Zn(OH)_2$, $Zn_5(OH)_8Cl_2 \cdot H_2O$, and Mg-Al layered double hydroxide (LDH) with the general formula, $M_xAl_y(A)_m(OH)_n \cdot zH_2O$ (where A and M represent an anion and a di-valent cation, respectively) [16,18,37]. As mentioned previously, the addition of Zn and Mg to the coating can help increase the corrosion resistance in a neutral aqueous solution, in such a way that several corrosion products with an inhibiting nature are formed preferentially on the surface at the early stages of corrosion. Among the products, Mg-Al LDH and $Zn_5(OH)_8Cl_2 \cdot H_2O$ can act as effective barriers for oxygen diffusion [38,39] and provide superior corrosion resistance in neutral aqueous solutions [38,39]. On the other hand, the formation or dissolution of other products can also help increase the corrosion resistance by stabilizing Mg-Al LDH and $Zn_5(OH)_8Cl_2 \cdot H_2O$. First, the formation of Mg-Al LDH, as shown in Figure 9d,f involves reactions (2), (4), (5), and (6).
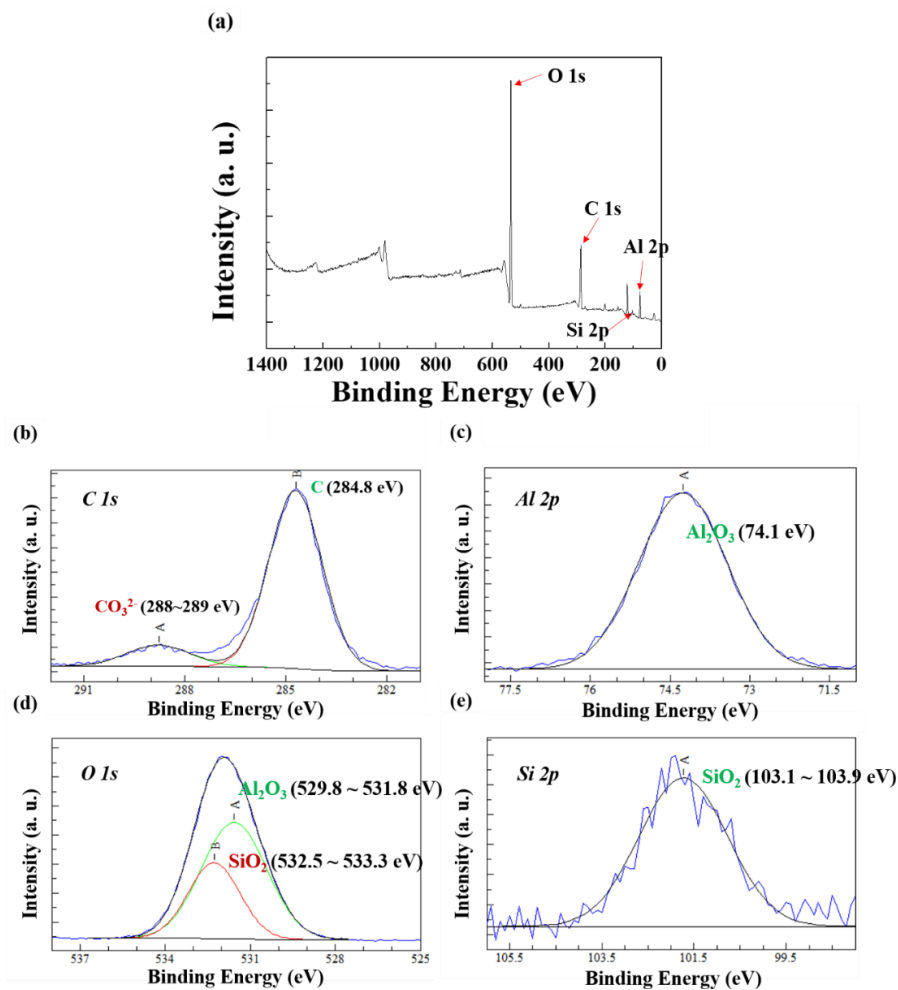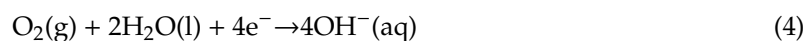
**Figure 8.** (**a**) XPS survey spectrum and (**b**–**e**) high-resolution spectra of the surface on AlSi-MC after the PS test.
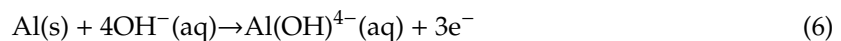
Oxygen reduction:

$$O_2(g) + 2H_2O(l) + 4e^- \rightarrow 4OH^-(aq) \tag{4}$$

Dissolution of alumina:

$$Al_2O_3(s) + 3H_2O(l) + 2OH^-(aq) \rightarrow 2Al(OH)^{4-}(aq) \tag{5}$$

Dissolution of metallic Al:

$$Al(s) + 4OH^-(aq) \rightarrow Al(OH)^{4-}(aq) + 3e^- \tag{6}$$

Reactions (5) and (6) can occur locally at the cathode area because of the instability of Al/Al$_2$O$_3$ at alkaline pH [16]. As a result, the formation reaction of LDH can proceed, as described below:

$$2Al(OH)^{4-}(aq) + 6Mg^{2+}(aq) + 8OH^-(aq) + CO_3{}^{2-}(aq) \rightarrow Mg_6Al_2(OH)_{16}CO_3(s) \tag{7}$$

The stability of LDH is dependent on the pH [40,41], and LDH can dissolve under weakly alkaline condition. On the other hand, the dissolution of LDH can be suppressed by the formation of a thin Mg(OH)$_2$ layer (reaction (8)), called the skin effect [15,37]:

$$Mg^+(aq) + 2OH^-(aq) \rightarrow Mg(OH)_2(s) \tag{8}$$
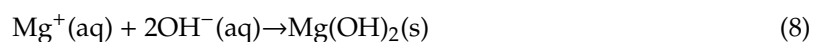
Second, the formation of $Zn_5(OH)_8Cl_2 \cdot H_2O$, as shown in Figure 9g, can be described below:

$$4ZnO(s) + Zn^{2+}(aq) + 5H_2O(l) + 2Cl^-(aq) \rightarrow Zn_5(OH)_8Cl_2 \cdot H_2O(s) \tag{9}$$
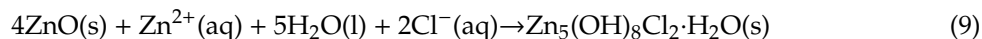
The presence of $Mg^{2+}$ supplied by reaction (2) can also delay the following reaction, which leads to slower dissolution kinetics of $Zn_5(OH)_8Cl_2 \cdot H_2O$. The formations of Mg-Al LDH and $Zn_5(OH)_8Cl_2 \cdot H_2O$ with high stability are the major mechanistic reasons for the higher corrosion resistance of AlSiZnMg in a neutral environment containing $Cl^-$. Nevertheless, the increased possibility of local corrosion of the AlSiZnMg sample cannot be excluded. In addition, its superiority and utility as a coated steel should also be evaluated after the electropainting process, which will be discussed in the following section.
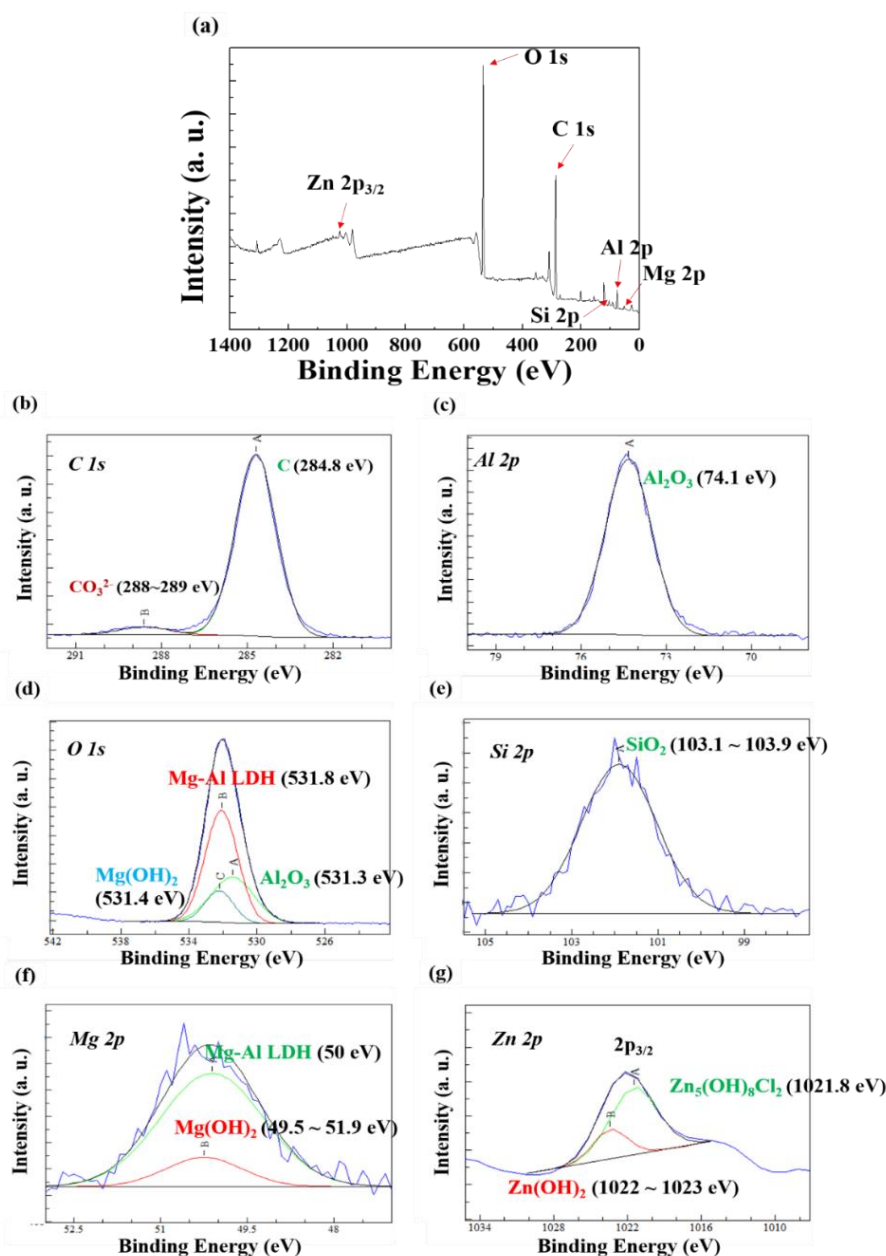


**Figure 9.** (**a**) XPS survey spectrum and (**b–g**) high-resolution spectra of the surface on AlSiZnMg-MC after PS test.

### 3.4. Surface Characteristics after Electropainting

Figure 10 presents the GDS depth profiles of AlSi-MC and AlSiZnMg-MC after the ED coating. In contrast to AlSi-MC, Zn(Mg)—based oxides were present on the outer surface of the ED-coated AlSiZnMg-MC. This suggests that the oxides remained on the outer surface, even after surface cleaning before the ED coating. As mentioned in the previous section, a stable thick MgO film cannot be formed in a minor fraction of Mg (0.5 wt %) in this coating system. An unstable oxide film on the surface may have weakened the adhesion between the inner metallic coating/outer ED coating and reduced the corrosion resistance.
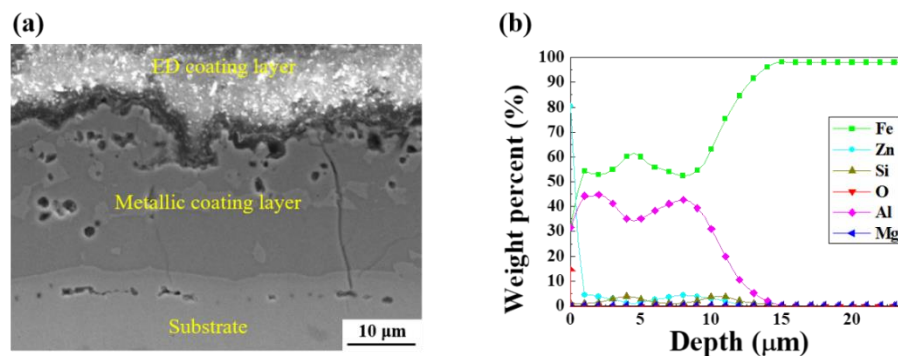


**Figure 10.** (**a**) Cross-sectional observation and (**b**) GDS depth profile of ED-treated AlSiZnMg-MC.

### 3.5. Corrosion Resistance Evaluations after Electropainting

Figure 11 shows the surface appearance of the ED-treated AlSi-MC (Figure 11a) and AlSiZnMg-MC (Figure 11b), after the accelerated corrosion test in reference to VDA 233-102 [12]. Considering the many test results presented above, it was expected that ED-treated AlSiZnMg-MC showed higher corrosion resistance when evaluated by an accelerated corrosion test. After the ED coating, however, its higher corrosion resistance was not observed clearly in that the damaged areas and extent of red rust formation on the scribed regions with an X between the two coated steels sheets became similar as the number of cycles increased. In addition, the surface morphologies of the two ED-coated steel samples that had been subjected to stone chipping and a subsequent corrosion test revealed even more severe surface degradation of ED-coated AlSiZnMg-MC. As shown in Figure 12, the size and number of surface blisters were larger on the ED-coated AlSiZnMg-MC. These blisters resulted from volumetric expansion caused by the formation of corrosion products on the steel substrate covered with a metallic coating layer. This suggests that the corrosive species are more able to permeate through the ED coating on AlSiZnMg-MC, and the electrochemical corrosion reactions occurred rapidly. The higher degradation by the corrosion reactions of ED coated AlSiZnMg-MC may be associated closely with the lower adhesion between the inner metallic coating/outer ED coating. As mentioned previously, the (Zn, Mg)-based oxide formed on AlSiZnMg can weaken the adhesion between the inner/outer coating layers, leading to delamination of the outer coating layer when attacked mechanically and chemically. This is supported by the lower coefficient of friction for the ED coating on AlSiZnMg-MC, which was measured by surface and interfacial cutting analysis, and was reported elsewhere [21]. Hence, the addition of Zn and Mg to the AlSi-based metallic coating does not always have beneficial effects on the corrosion resistance when the metallic-coated steels are coated additionally with ED paint. These results provide useful insights into the development of coated steel sheets used in automotive industries. Nevertheless, further technical research on optimizing the compositions of Zn and/or Mg alloying that provides sacrificial corrosion protection to the AlSi coated steel while reducing the possibility of local corrosion and securing superior corrosion resistance even after additional ED coating will be needed.
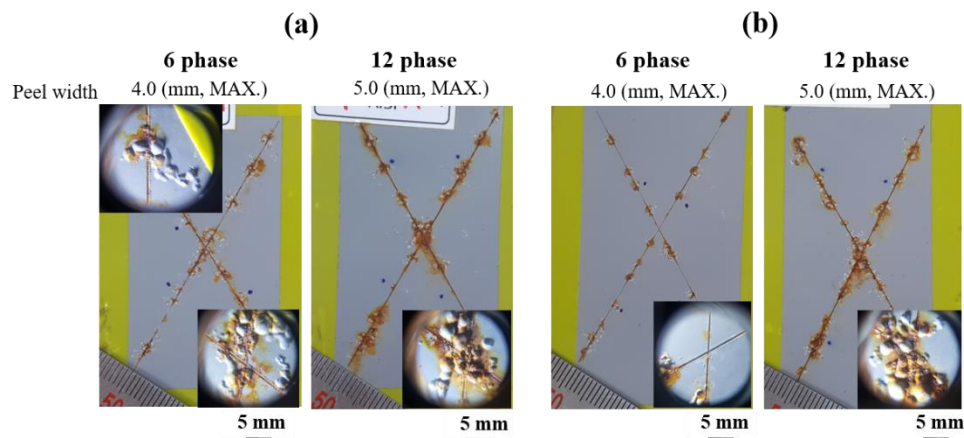
**Figure 11.** Surface appearance of electrodeposited (ED)-treated (**a**) AlSi-MC and (**b**) AlSiZnMg-MC, which had been scratched with an "×" incision, after the accelerated corrosion test.
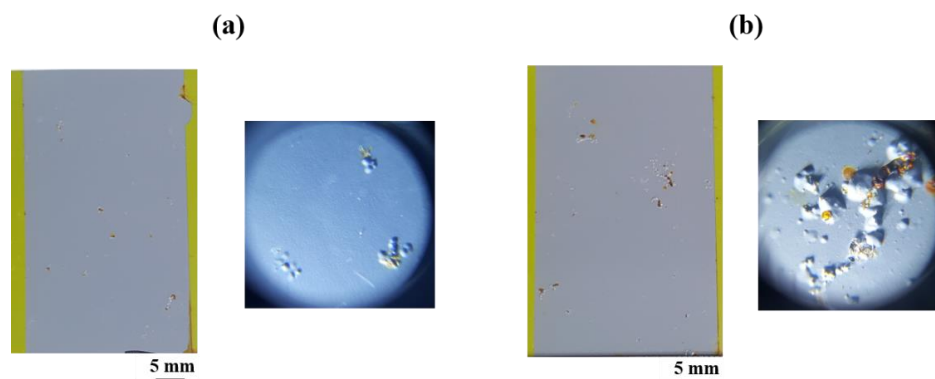


**Figure 12.** Surface appearance of ED-treated (**a**) AlSi-MC and (**b**) AlSiZnMg-MC, which had been collided with fine stone chips, after the accelerated corrosion test.

## 4. Conclusions

The influence of the combined addition of Mg and Zn on the microstructure and corrosion resistance of AlSi-based coatings for steel sheets was investigated using a range of analytical and experimental techniques. In particular, the corrosion resistance was also evaluated after ED coating on the metallic coated steel sheets. The major findings can be summarized as follows:

1. The two types of AlSi-based coating (AlSi-MC and AlSiZnMg-MC) were composed mainly of an Al matrix with two (Al,Fe,Si)-rich intermetallic phases. The compositional features were different in that the intermetallic phases of $MgZn_2$ and $Mg_2Si$ existed only in AlSiZnMg-MC covered with a thin outermost layer of (Zn, Mg)-based oxide.

2. The active phases formed in AlSiZnMg-MC, such as $Mg_2Si$ and $MgZn_2$, can decrease the corrosion potential. The preferential dissolution of Mg and Zn from the active phases can lead to rapid coverage of the coating surface by the precipitation of corrosion products with a protective nature, resulting in a much smaller current density for both anodic and cathodic reactions. On the other hand, the polarization curve of AlSiZnMg-MC showed many fluctuations, which may be closely associated with localized corrosion caused by the non-uniform distribution of MgO or the selective dissolution of Mg from $Mg_2Si$ phases in the coating.

3. Compared to the case of the AlSi-MC, XPS showed that the surface of AlSiZnMg-MC was composed of a wider variety of corrosion products, including $Al_2O_3$, $Mg(OH)_2$, $SiO_2$, $Zn(OH)_2$, $Zn_5(OH)_8Cl_2 \cdot H_2O$, and Mg-Al LDH. Among the products, the presence of $Zn_5(OH)_8Cl_2 \cdot H_2O$

and Mg-Al LDH, stabilized by Mg(OH)$_2$, is the major mechanistic reason for the higher corrosion resistance of AlSiZnMg-MC.

4. In contrast to the corrosion resistance of metallic coatings, ED-coated AlSiZnMg-MC exhibited more severe surface degradation after the accelerated corrosion tests. The non-uniform formation of Mg-based oxide over the AlSiZnMg-MC can weaken the adhesion between the inner metallic coating/outer ED coating. Hence, the corrosive species are more able to permeate through the ED coating on AlSiZnMg-MC, and the electrochemical corrosion reactions occurred rapidly. Therefore, further optimization of the alloy contents in AlSi-based coatings needs to be investigated.

**Author Contributions:** Conceptualization, W.S.Y. and S.J.K.; methodology, S.O.K., W.S.Y., and S.J.K.; investigation, S.O.K., W.S.Y., and S.J.K.; data curation, S.O.K., W.S.Y., and S.J.K., writing—original draft preparation, S.O.K. and S.J.K. All authors have agreed to the published version of the manuscript.

**Conflicts of Interest:** The authors declare no conflict of interest.

## References

1. Ahmad, Z. *Principles of Corrosion Engineering and Corrosion Control*, 2nd ed.; Butterworth-Heinemann: London, UK, 2006.
2. Forsyth, M.; Hinton, B. *Rare Earth-Based Corrosion Inhibitors*; Woodhead Publishing: Cambridge, UK, 2014.
3. Schürz, S.; Luckeneder, G.H.; Fleischanderl, M.; Mack, P.; Gsaller, H.; Kneissl, A.C.; Mori, G. Chemistry of corrosion products on Zn-Al-Mg alloy coated steel. *Corros. Sci.* **2010**, *52*, 3271–3279. [CrossRef]
4. Thebault, F.; Vuillemin, B.; Oltra, R.; Ogle, K.; Allely, C. Investigation of self-healing mechanism on galvanized steels cut edges by coupling SVET and numerical modeling. *Electrochim. Acta* **2008**, *53*, 5226–5234. [CrossRef]
5. Ogle, K.; Morel, S.; Jacquet, D. Observation of self-healing functions on the cut edge of galvanized steel using SVET and pH microscopy. *J. Electrochem. Soc.* **2006**, *153*, B1–B5. [CrossRef]
6. Zeng, F.; Wei, Z.; Li, C.; Tan, X.; Zhang, Z. Corrosion mechanism associated with Mg$_2$Si and Si particles in Al–Mg–Si alloys. *Trans. Nonferrous Met. Soc. China* **2011**, *21*, 2559–2567. [CrossRef]
7. Zhang, Y.S.; Zhu, X.M. Electrochemical polarization and passive film analysis of austenitic Fe–Mn–Al steels in aqueous solutions. *Corros. Sci.* **1999**, *41*, 1817–1833. [CrossRef]
8. Bobby Kannan, M.; Singh Raman, R.K.; Khoddam, S. Comparative studies on the corrosion properties of a Fe–Mn–Al–Si steel and an interstitial-free steel. *Corros. Sci.* **2008**, *50*, 2879–2884. [CrossRef]
9. Panossian, Z.; Mariaca, L.; Morcillo, M.; Flores, S.; Rocha, J.; Peña, J.J.; Herrera, F.; Corvo, F.; Sanchez, M.; Rincon, O.T.; et al. Steel cathodic protection afforded by zinc, aluminum and zinc/aluminium alloy coatings in the atmosphere. *Surf. Coat. Technol.* **2005**, *190*, 244–248. [CrossRef]
10. Han, S.; Li, H.; Wang, S.; Jiang, L.; Liu, X. Influence of silicon on hot-dip aluminizing process and subsequent oxidation for preparing hydrogen/tritium permeation barrier. *Int. J. Hydrog. Energy* **2010**, *35*, 2689–2693. [CrossRef]
11. Cheng, W.J.; Wang, C.J. Microstructural evolution of intermetallic layer in hot-dipped aluminide mild steel with silicon addition. *Surf. Coat. Technol.* **2011**, *205*, 4726–4731. [CrossRef]
12. Allely, C.; Dosdat, L.; Clauzeau, O.; Ogle, K.; Volovitch, P. Anticorrosion mechanisms of aluminized steel for hot stamping. *Surf. Coat. Technol.* **2014**, *238*, 188–196. [CrossRef]
13. Szklarska-Smialowska, Z. Pitting corrosion of Al. *Corros. Sci.* **1999**, *41*, 1743–1767. [CrossRef]
14. Vargel, C. *Corrosion of Aluminium*; Elsevier: Oxford, UK, 2004.
15. Salgueiro Azevedo, M.; Allely, C.; Ogle, K.; Volovitch, P. Corrosion mechanisms of Zn (Mg,Al) coated steel: The effect of HCO$_3^-$ and NH$_4^+$ ions on the intrinsic reactivity of the coating. *Electrochim. Acta* **2015**, *153*, 159–169. [CrossRef]

16.  Volovitch, P.; Vu, T.N.; Allély, C.; Abdel Aal, A.; Ogle, K. Understanding corrosion via corrosion product characterization: II. Role of alloying elements in improving the corrosion resistance of Zn–Al–Mg coatings on steel. *Corros. Sci.* **2011**, *53*, 2437–2445. [CrossRef]

17.  Prosek, T.; Larché, N.; Vlot, M.; Goodwin, F.; Thierry, D. Corrosion performance of Zn–Al–Mg coatings in open and confined zones in conditions simulating automotive applications. *Mater. Corros.* **2010**, *61*, 412–420. [CrossRef]

18.  Nicarda, C.; Allély, C.; Volovitch, P. Effect of Zn and Mg alloying on microstructure and anticorrosion mechanisms of Al-Si based coatings for high strength steel. *Corros. Sci.* **2019**, *146*, 192–201. [CrossRef]

19.  Hwang, Y.; Lee, C.W.; Shin, G.Y.; Yoo, J.H.; Choi, M. Study of the corrosion behavior, liquid metal embrittlement and resistance spot weldability of galvannealed hot stamping steel. *Korean J. Met. Mater.* **2019**, *57*, 193–201. [CrossRef]

20.  Kharitonov, D.S.; Örnek, C.; Claesson, P.M.; Sommertune, J.; Zharskii, I.M.; Kurilo, I.I.; Pan, J. Corrosion inhibition of aluminum alloy AA6063-T5 by vanadates, microstructure characterization and corrosion analysis. *J. Electrochem. Soc.* **2018**, *165*, C116–C126. [CrossRef]

21.  Yang, W.S.; Ahn, S.H.; Kim, S.J. Effects of Zn and Mg addition to AlSi metallic coating for hot stamping steel. In *Hyundai Steel Technical Report*; Hyundai Steel Company: Chungnam, Korea, 2019; Volume 7, pp. 12–17. ISSN 2288-6990.

22.  Susi, T.; Pichler, T.; Ayala, P. X-ray photoelectron spectroscopy of graphitic carbon nanomaterials doped with heteroatoms. *Beilstein J. Nanotechnol.* **2015**, *6*, 177–192. [CrossRef]

23.  *Standard Test Method for Evaluation of Painted or Coated Specimens Subjected to Corrosive Environments*; ASTM D1654–08; ASTM International: West Conshohocken, PA, USA, 2016.

24.  *Standard Test Method for Chipping Resistance of Coatings*; ASTM D3170; ASTM International:  West Conshohocken, PA, USA, 2014.

25.  Wang, C.J.; Chen, S.M. The high-temperature oxidation behavior of hot-dipping Al–Si coating on low carbon steel. *Surf. Coat. Technol.* **2006**, *200*, 6601–6605. [CrossRef]

26.  Jo, K.R.; Cho, L.; Sulistiyou, D.H.; Seo, E.J.; Kim, S.W.; De Cooman, B.C. Effects of Al-Si coating and Zn coating on the hydrogen uptake and embrittlement of ultra-high strength press-hardened steel. *Surf. Coat. Technol.* **2019**, *374*, 1108–1119. [CrossRef]

27.  Grigorieva, R.; Drillet, P.; Mataigne, J.M.; Redjaïmia, A. Phase transformations in the Al-Si coating during the austenitization step. *Solid State Phenom.* **2011**, *172–174*, 784–790. [CrossRef]

28.  Maitra, T.; Gupta, S.P. Intermetallic compound formation in Fe–Al–Si ternary system:  Part II. *Mater. Charact.* **2003**, *49*, 293–311. [CrossRef]

29.  Bruschi, S.; Ghiotti, A. *Comprehensive Materials Processing*; Elsevier: Amsterdam, The Netherlands, 2014.

30.  Windmann, M.; Röttger, A.; Theisen, W. Phase formation at the interface between a boron alloyed steel substrate and an Al-rich coating. *Surf. Coat. Technol.* **2013**, *226*, 130–139. [CrossRef]

31.  Kobayashi, S.; Yakou, T. Control of intermetallic compound layers at interface between steel and aluminum by diffusion-treatment. *Mater. Sci. Eng. A* **2002**, *338*, 44–53. [CrossRef]

32.  Cho, Y.R.; Kim, T.H.; Park, S.H.; Baek, E.R. Aluminum-Plated Steel Sheet Having Superior Corrosion Resistance, Hot Press Formed Product Using the Same, and Method for Production Thereof.  European Patent WO/2010/079995, 15 July 2010.

33.  Li, Q.; Zhao, Y.Z.; Luo, Q.; Chen, S.L.; Zhang, J.Y.; Chou, K.C. Experimental study and phase diagram calculation in Al–Zn–Mg–Si quaternary system. *J. Alloy. Compd.* **2010**, *501*, 282–290. [CrossRef]

34.  Samsonov, G.V. *The Oxide Handbook*, 2nd ed.; IFI/Plenum: New York, NY, USA, 1973.

35.  Lee, J.W.; Park, B.R.; Oh, S.Y.; Yun, D.W.; Hwang, J.K.; Oh, M.S.; Kim, S.J. Mechanistic study on the cut-edge corrosion behaviors of Zn-Al-Mg alloy coated steel sheets in chloride containing environments. *Corros. Sci.* **2019**, *160*, 108170. [CrossRef]

36.  Volovitch, P.; Barrallier, L.; Saikaly, W. Microstructure and corrosion resistance of Mg alloy ZE41 with laser surface cladding by Al–Si powder. *Surf. Coat. Technol.* **2008**, *202*, 4901–4914. [CrossRef]

37.  Salgueiro Azevedo, M.; Allely, C.; Ogle, K.; Volovitch, P. Corrosion mechanisms of Zn (Mg,Al) coated steel: 2.  The effect of Mg and Al alloying on the formation and properties of corrosion products in different electrolytes. *Corros. Sci.* **2015**, *90*, 482–490. [CrossRef]

38.  Hosking, N.C.; StrÖm, M.A.; Shipway, P.H.; Rudd, C.D. Corrosion resistance of zinc–magnesium coated steel. *Corros. Sci.* **2007**, *49*, 3669–3695. [CrossRef]

39. Ishizaki, T.; Kamiyama, N.; Watanabe, K.; Serizawa, A. Corrosion resistance of Mg(OH)$_2$/Mg–Al layered double hydroxide composite film formed directly on combustion-resistant magnesium alloy AMCa602 by steam coating. *Corros. Sci.* **2015**, *92*, 76–84. [CrossRef]

40. Wu, L.; Pan, F.; Liu, Y.; Zhang, G.; Tang, A.; Atrens, A. Influence of pH on the growth behavior of Mg–Al LDH films. *Surf. Eng.* **2017**, *34*, 674–681. [CrossRef]

41. Zhang, F.; Zhang, C.L.; Song, L.; Zeng, R.C.; Liu, Z.G.; Cui, H.Z. Corrosion of in-situ grown MgAl-LDH coating on aluminum alloy. *Trans. Nonferrous Met. Soc. China* **2015**, *25*, 3498–3504. [CrossRef]